

Mechanical, Electrostatic, and Electromagnetic Manipulation of Microobjects and Nanoobjects in Electron Microscopes

Andrey I. Denisyuk¹, Alexey V. Krasavin², Filipp E. Komissarenko¹ and Ivan S. Mukhin^{1,3}

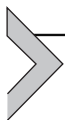
¹St. Petersburg National Research University of Information Technologies, Mechanics, and Optics (ITMO University), 49 Kronverksky, 197101 St. Petersburg, Russia

²Department of Physics, King's College London, Strand, London WC2R 2LS, United Kingdom

³St. Petersburg Academic University—Nanotechnology Research and Education Centre of the Russian Academy of Sciences, 8/3 Khlopina St., 195220 St. Petersburg, Russia

Contents

1. Introduction	101
2. Overview of Forces Acting on a Particle in an Electron Microscope	104
2.1 Introduction	104
2.2 Adhesion of Particles in Vacuum Conditions	104
2.3 Electrostatic Interaction Between Objects Charged due to Electron Irradiation	106
2.4 Electromagnetic Force Exerted on a Particle by Fast-Passing Electrons	109
3. Mechanical Manipulation	114
3.1 Introduction	114
3.2 Commercial Micromanipulators	115
3.3 Handling Microobjects and Nanoobjects and Investigation of Their Mechanical Properties	117
4. Electrostatic Manipulation	124
5. Electromagnetic Manipulation	131
6. Conclusion	135
Acknowledgments	136
References	136



1. INTRODUCTION

Nanofabrication methods rely on three basic approaches. One approach, called *top-down*, assumes the fabrication of nanoscale structures from a macroscale object. Typical examples of this method are various

lithographic techniques (photolithography, electron beam lithography, focused ion beam etc.). The second approach is called *bottom-up*; here, nano-objects are created by molecular assembly, as in physical and chemical vapor deposition or colloidal chemistry. The third approach is micromanipulation, which is based on the transportation of existing objects (fabricated by other techniques) for the purpose of their investigation, or fabrication of complex structures assembled from basic ones. Micromanipulation techniques can be divided into two groups: manipulation of multiple objects by such techniques as electrophoresis, magnetophoresis, and hydrodynamics; and manipulation of individual microobjects and nanoobjects. The latter is usually based on various microscopic techniques described below.

Optical (or laser) tweezers, introduced by [Ashkin \(1970\)](#), is supposedly the first method of micromanipulation of individual particles. The underlying physical mechanisms of this phenomenon are now well understood (see, for instance, [Neuman & Block, 2004](#) and references therein). However, the limitation of this technique is the size of the transported objects, which should be comparable to the wavelength of light (i.e., not much less than a micrometer).

Other methods for individual particle manipulation rely on using scanning probe microscopes. In one of these, the manipulation mechanism is based on mechanical ([Sitti & Hashimoto, 2000](#)) or electrostatic ([Grobelny et al., 2006](#); [Kim et al., 2011](#)) interaction between the probe and the objects. Also, an object can be glued ([Ducker, Senden, & Pashley, 1991](#)) or chemically bound ([Höppener & Novotny, 2008](#)) to the probe tip. Manipulation in a scanning probe microscope allows for handling particles as small as 5–15 nm in diameter ([Kim et al., 2011](#)). However, this kind of manipulation has a limitation: the same probe is used for manipulation and imaging purposes afterwards. So this strategy is not real time, but what is called “move and look.” The other shortcomings are that scanning probe microscopes do not allow the visualization of complex structures with high aspect ratios and the modification of the probe during the manipulation process.

The last group of micromanipulation methods is related to manipulation in scanning and transmission electron microscopes (SEMs and TEMs), which is the topic of this chapter. Electron microscopes do not have the limitations that optical tweezers or scanning probe microscopes have. Micromanipulation in SEMs and TEMs allows for handling the individual microobjects and nanoobjects with nanometer precision while the process and the result of the manipulation can be seen in high resolution in real time. In this chapter, we divided the micromanipulation techniques

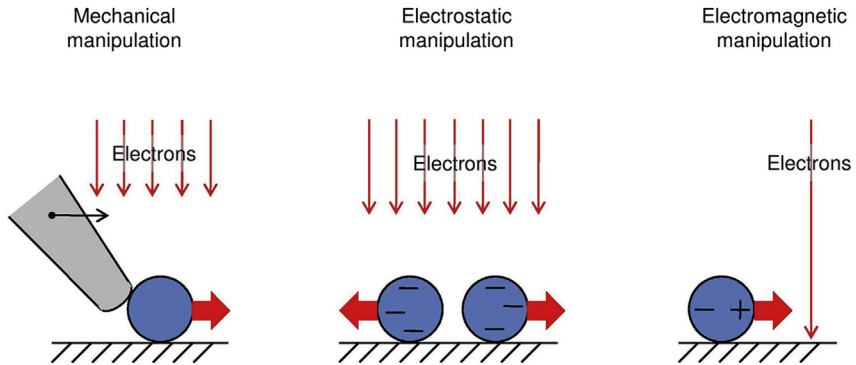


Figure 3.1 Schematic illustration of micromanipulation techniques in electron microscopes: (left) mechanical manipulation (where a micromanipulator is employed, while an electron microscope is used for imaging purposes); (center) electrostatic manipulation (where an electron beam charges particles, which results in attractive or repulsive forces); and (right) electromagnetic manipulation (where an electron beam induces an electromagnetic force exerted on the particle). (See the color plate.)

involving electron microscopes into three main groups (illustrated schematically in [Figure 3.1](#)):

- **Mechanical manipulation.** This approach relies on using a number of micromanipulators installed in the chamber of an electron microscope. Here, the manipulation is based on mechanical contact or adhesion interaction between a probe tip of a micromanipulator and an object.

In addition to this technique, there are noncontact manipulation methods based on intrinsic properties of an electron beam. These are described next

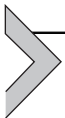
- **Electrostatic manipulation.** Here, the manipulation is based on electrostatic interaction between objects charged under electron beam illumination.
- **Electromagnetic manipulation.** This method is based on the influence of an electromagnetic force created by a beam of passing electrons.

Mechanical manipulation is a well-developed technique, and there is a great many publications in the literature on this topic. Thus, in this chapter, we tried to relate similar approaches, provide references, and focus mostly on several outstanding applications, such as the investigation of mechanical properties of microobjects and nanoobjects. On the other hand, electrostatic and electromagnetic manipulation techniques are far less known. Electrostatic motion of charged objects has been observed in the past; however, guided electrostatic manipulation is not widely used. Electromagnetic manipulation was experimentally demonstrated just a few years ago. The

number of publications related to electrostatic and electromagnetic manipulation is very limited. Therefore, here, our review strategy is different: we pay more attention to each publication.

It should be noted that there are also other physical mechanisms of particle manipulation in electron microscopes. For instance, heating of clusters by an electron beam may cause their motion (Williams, 1987) and coalescence (van Huis *et al.*, 2008). Activation of surface bonds by the electron beam also can cause clusters to move (Cretu *et al.*, 2012). Non-Brownian motion of particles was also observed in liquid cells under electron irradiation (Chen & Wen, 2012; Chen *et al.*, 2013). Some studies (e.g., Zheng *et al.*, 2008) describe motion phenomena observed in electron microscopes; however, this motion is not related to a micromanipulator or to the influence of the electron beam. All these experimental results demonstrate a mere particle movement rather than a guided manipulation, and thus these mechanisms will not be taken into account here.

We begin by considering various forces that act on a particle in an electron microscope.



2. OVERVIEW OF FORCES ACTING ON A PARTICLE IN AN ELECTRON MICROSCOPE

2.1 Introduction

Contrary to macroscale, the force of gravity has a very minor impact when the size of an object approaches microscale and nanoscale. At the same time, other forces take over, such as van der Waals forces, external and internal magnetic and electrostatic forces, and capillary forces (Min *et al.*, 2008).

Now, let us consider the forces acting on a particle in electron microscopes. We will examine only a classical arrangement where a particle sits on a substrate, although presently, various liquid cell techniques have become popular in SEMs and TEMs (some aspects of these methods are reviewed in the sections “Electrostatic Manipulation” and “Electromagnetic Manipulation,” later in this chapter). We start with the adhesion of a particle to a substrate in vacuum conditions.

2.2 Adhesion of Particles in Vacuum Conditions

The van der Waals attraction between two undeformed spherical particles can be calculated using a simple formula derived by Hamaker (1937):

$$F_{\text{vdW}} = \frac{A}{6} \frac{R_1 R_2}{R_1 + R_2} \frac{1}{z_0^2}, \quad (1)$$

where R_1 and R_2 are the radii of the particles, A is the Hamaker constant for the interacting materials, and z_0 is the separation distance between the particle and the substrate. For most materials, the Hamaker constant is on the order of $10^{-20} - 10^{-19}$ J for interactions in vacuum and about 10 times less than this value for interactions in water. Hamaker constants for some materials can be found in Bergstrom (1997). The separation in the idealized conditions of atomically smooth surface contact is just 3–4 Å. However, the surface roughness of real contacting solids increases the equivalent separation between them (Hu *et al.*, 2010). Here, we calculated the van der Waals attraction force between two spherical particles using Eq. (1) and took $A = 5 \cdot 10^{-20}$ J and $z_0 = 4$ Å. The resulting force is plotted against the particle radius shown in Figure 3.2.

In the case of the deformation of the contacting objects, we need to take into account the contact area, which is assumed to be flat. The attraction force per unit area between two flat surfaces is given by $A/6\pi z_0^3$ (Hamaker,

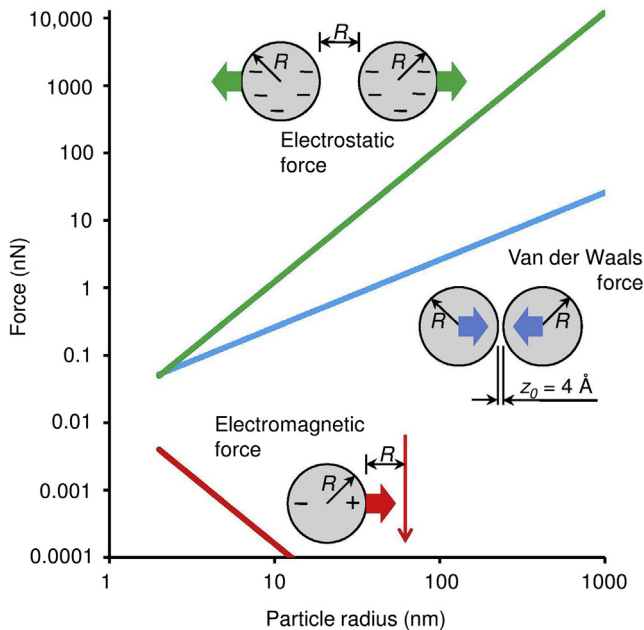


Figure 3.2 Comparison of forces acting on a small spherical particle plotted against a particle radius: van der Waals force between two spheres, Coulomb repulsion force between two charged particles (with separation between them equal to R), and peak electromagnetic force exerted on a particle by a single passing electron (again, with separation equal to R). Forces for very small particles ($R < 2$ nm) are not shown because simplified models used in these calculations would not be valid in such a case. (See the color plate.)

1937). Then the attraction between a deformed spherical particle and a flat substrate (Hu *et al.*, 2010), for instance, can be found as

$$F_{\text{vdW}} = \frac{AR}{6z_0^2} \left(1 + \frac{a^2}{Rz_0} \right), \quad (2)$$

where a is the contact radius of the spherical particle after its deformation. Other scenarios for contact mechanics between the deformed solids can be treated using the famous JKR model (Johnson, Kendall, & Roberts, 1971) or DMT model (Derjaguin, Muller, & Toporov, 1975).

This scenario describes the load needed to tear off a particle from a substrate; however, it is also possible to have a sliding motion of a particle over a substrate. The value for the friction force is given by $F_{\text{frict}} = \tau \cdot 2\pi a^2$, where a is the contact radius and τ is the interfacial shear strength with a typical value in the range of 10^7 – 10^9 Pa (Carpick & Salmeron, 1997). Thus, the friction force in the nanoscale is proportional to the contact area, which differs from the situation in the macroscale.

It should be noted that the way by which the particle was deposited on the substrate can have a crucial influence on the adhesion (Hu *et al.*, 2010). For instance, if the particle was deposited from a liquid suspension by drop-casting and desiccation, then a liquid meniscus is formed between the particle and the flat substrate. It causes a capillary force, which is even stronger than the van der Waals force. The capillary force significantly deforms the particle, and the contact area increases. Being placed in vacuum conditions, the liquid meniscus evaporates and the capillary force disappears; however, the deformation of particles remains, and adhesion in vacuum will be generally the same as it was in air when the capillary force took place (Hu *et al.*, 2010).

In addition, the wet deposition may cause condensation of impurities. Contreras-Naranjo and Ugaz (2013) provided a good illustration of such capillary condensation dynamics (Figure 3.3). Obviously, this also strongly increases the adhesion. Various cases of the contact interface are schematically illustrated in Figure 3.4. As will be shown in the section “Electrostatic Interaction Between Objects Charged due to Electron Irradiation,” later in this chapter, micromanipulation systems are able to supply significant forces, which can easily overcome the adhesion of microobjects and nanoobjects.

2.3 Electrostatic Interaction Between Objects Charged due to Electron Irradiation

Charging of dielectric (or ungrounded conductive) objects due to electron bombardment causes electrostatic interaction between them. This can create

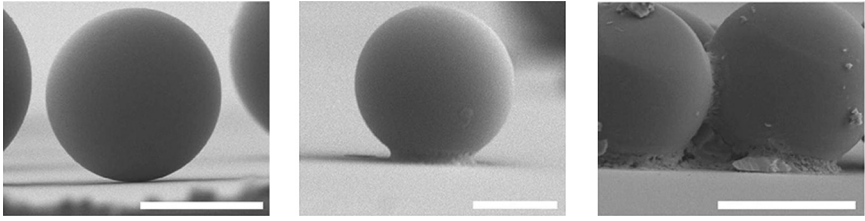


Figure 3.3 SEM images illustrating particle-substrate contact in the cases of dry deposition (left) and wet deposition (center and right) of polystyrene particles on a glass substrate. Wet deposition usually causes the accumulation of impurities underneath the particle. *Reproduced with permission from Contreras-Naranjo and Ugaz (2013). Copyright by Nature Publishing Group.*

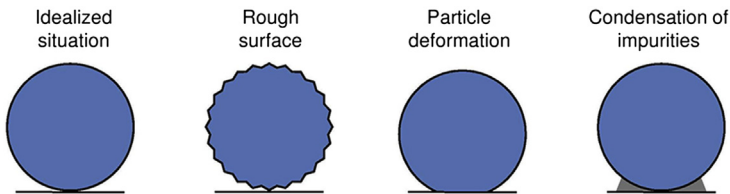


Figure 3.4 Adhesion between a spherical particle and a substrate for various contact interfaces. (See the color plate.)

significant adhesion or repulsion. The physics of charging a dielectric specimen due to electron irradiation is more complex than it looks at first. One can find comprehensive investigations of this phenomenon in [Cazaux \(2004\)](#) or [Egerton, Li, and Malac \(2004\)](#) and references therein.

Scattering of primary electrons during electron-specimen interaction consists of elastic and inelastic collisions. Elastic collision of the primary electrons with specimen atomic nuclei causes deflection of their initial trajectories and formation of backscattered electrons, which are emitted out of the specimen. Ionization of specimen atoms during inelastic collisions leads to the formation of secondary electrons; some of them may leave the specimen during secondary electron emission. Those primary electrons, which lost all their kinetic energy during the collision but did not escape the specimen, become absorbed and charge the specimen negatively. One should note that in the case of low-energy primary electrons, the total charge of the object can be close to zero (or even positive) because the absorbed charge is compensated by higher yield of the secondary electrons. These effects can be illustrated in the following equation:

$$I_b = I_b\eta + I_b\delta + \partial Q/\partial t, \quad (3)$$

where I_b is the current of the primary electron beam, η is the backscattering coefficient, δ is the secondary electron yield, and $\partial Q/\partial t$ is the increase in the accumulated charge. The values for backscattering coefficient and secondary electron yield can be obtained by Monte-Carlo simulation.

However, the entire phenomenon is more complex. The negative charge formed by the trapped electrons can significantly affect the landing energies and trajectories of the primary electrons, as well as the secondary electron emission yield. Thus, the accumulation of the charge is a nonlinear process, and discharge effects also should be taken into account.

Moreover, charging of specimens due to electron irradiation depends not only on specimen electrical properties and primary electron energy, but also on the size and shape of the specimen objects. Let us consider different situations for a dielectric particle sitting on a conductive substrate (Figure 3.5). If the particle is big enough, then the primary electrons are stopped in it, so the particle will be charged negatively. In the case of a small particle, through which primary electrons predominantly pass, the particle will be charged positively because the secondary electron emission will still take place. In

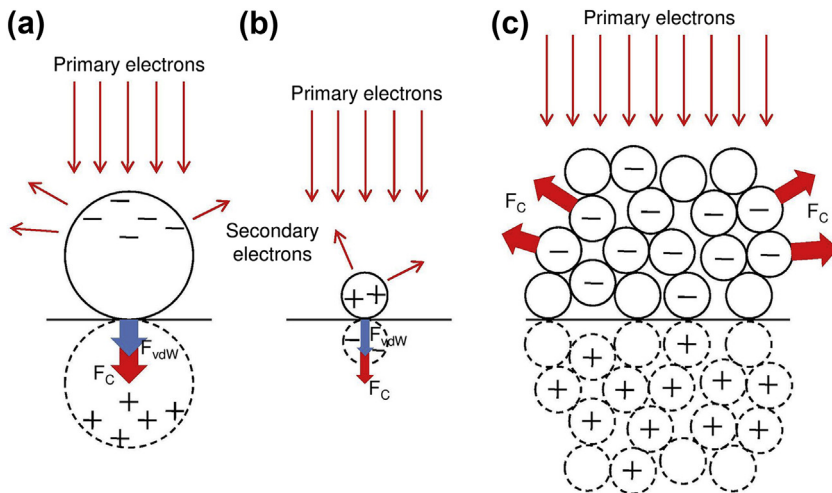


Figure 3.5 Different cases of charging under electron illumination and the resulting adhesion/repulsion for dielectric particles sitting on a conductive substrate (F_{vdW} = van der Waals force; F_C = Coulomb force). (a) A big particle will accumulate a negative charge, which causes increased adhesion to the substrate due to attraction between the charge and its mirror image; (b) a small particle most probably will accumulate a positive charge, and attraction and increased adhesion will take place; (c) small particles piled on top of each other will be charged negatively, which will cause repulsion between them. (See the color plate.)

both cases, the charge accumulated by the particles will form a mirror image with an opposite sign in the substrate, increasing the particle–substrate attraction. However, if small particles are piled on top of each other, then negative charging will take place, which will cause repulsion between the neighboring particles that might be stronger than their adhesion. Some issues regarding the adhesion of micrometer-sized polymer spheres in an SEM were experimentally investigated by Miyazaki *et al.* (2000a, b), who detected an increase of adhesion for micrometer-sized polymer spheres illuminated by electrons (see the section “Handling micro- and nanoobjects and investigation of their mechanical properties”, below in this chapter)

Thus, the charge accumulated by an object under electron beam illumination can take various values and even signs. Now, let us estimate the maximum electrostatic force between two charged spherical particles separated by a distance equal to a particle radius. We assumed that the charge accumulated by each particle would reach the value at which the electric field at the particle surface is 10^9 V/m (higher values would cause discharge due to the field emission effect). The force calculated via Coulomb’s law plotted against the particle radius was shown previously in Figure 3.2. One can compare this Coulomb force with the van der Waals force and find that the electrostatic interaction can easily be stronger than adhesion forces, especially for large particles.

2.4 Electromagnetic Force Exerted on a Particle by Fast-Passing Electrons

A fast electron is a source of time-dependent gradient electromagnetic field, possessing a wide range of frequency components in its Fourier spectrum. Flying in the vicinity of a metallic or dielectric particle, this field polarizes it. The resulting, generally multipole, surface charge excitations interact with the source field, exerting a sharp impulse of electromagnetic force as the electron flies by. Thus, if a focused electron beam approaches the particle, the latter experiences a quasi-continuous, time-averaged force, which can be used for its trapping or manipulation.

The problem of momentum transfer to small particles by passing electrons was theoretically investigated by García de Abajo (2004). It was found that the particle momentum change is given by the following frequency integral:

$$\Delta \mathbf{p} = \int_0^{\infty} \mathbf{F}(\omega) d\omega, \quad (4)$$

where

$$\mathbf{F}(\omega) = \frac{1}{4\pi^2} \text{Re} \left\{ \oint_S d\mathbf{s} (\mathbf{E}(\mathbf{s}, \omega) (\mathbf{E}(\mathbf{s}, \omega) \cdot \hat{\mathbf{n}})^* + \mathbf{H}(\mathbf{s}, \omega) \times (\mathbf{H}(\mathbf{s}, \omega)^* \cdot \hat{\mathbf{n}})^* - \frac{\hat{\mathbf{n}}}{2} (|\mathbf{E}(\mathbf{s}, \omega)|^2 + |\mathbf{H}(\mathbf{s}, \omega)|^2)) \right\} \quad (5)$$

defines the relative input of the Fourier components of the total electromagnetic field, including an external field (produced by the electron) and an induced field (due to multipole excitation in the particle). Here, the integration is done over the nanoparticle surface, and $\hat{\mathbf{n}}$ is the surface normal. The total field can be found expressing the source field in the basis of spherical functions with an origin at the nanoparticle center and matching them with the induced multipole fields via standard boundary conditions. The derived formalism was applied to both dielectric (Al_2O_3) and metallic (Ag) nanoparticles. In both nanoparticle types, and for all the distances between the center of the particle and the beam (impact parameters), the longitudinal component of the momentum supplied to the particle, parallel to the velocity of the electrons, always points in the same direction as the latter. This means that the particle is pushed along the direction of the beam. The magnitude of the supplied momentum in this direction (and therefore the force experienced by the particle) drastically increases as the impact parameter becomes smaller.

The situation is more interesting, though, for the transverse component of the supplied momentum, perpendicular to the beam direction. For the alumina nanoparticle, for all the impact parameters, this component is directed toward the beam. It also rapidly increases with the decrease of the impact parameter and tends toward zero as the parameter decreases. Interestingly, the latter happens at a much slower rate than for the longitudinal component; therefore, at larger impact parameters, the transverse force component dominates. For the smallest particle considered ($r = 10$ nm), the monotonic increase of this momentum component at small impact parameters (~ 50 nm) is perturbed. For metallic nanoparticles, however, in the analogous situation, the transverse force even changes sign. So one can conclude that while at large impact parameters, the metallic particle is attracted to the electron beam, at small impact parameters, the particle is actually pushed away from it. The domination of the transverse component at large impact parameters happens for metallic particles as well. At the same

time, the ratio between the components in the limit of nanometer impact parameters depends on the particle type and size [c.f. the data from [García de Abajo \(2004\)](#) and [Reyes-Coronado *et al.* \(2010\)](#)]. In addition, for both particles, the passing electron induces a torque on a particle that makes it rotate.

A comprehensive review of the physics of force formation in the case of metallic nanoparticles was given by [Reyes-Coronado *et al.* \(2010\)](#). In particular, the mechanism reveals itself when the dielectric response function of the material is defined by the Drude model (parameters corresponding to aluminium were considered). As previously noted, the electromagnetic field of a fast (> 100 keV) electron possesses in its Fourier spectrum the whole range of frequencies from 0 to tens of electronvolts, matching the energies of the plasmonic multipole resonances in the nanoparticle. Therefore, certain frequency components of this spectrum resonantly excite the latter, which results in an inevitable transfer of momentum from the electron to the particle. The higher-frequency components are present mostly in the vicinity of the electron trajectory (since they have more rapid evanescent decay), while the lower-frequency components penetrate into space for greater distances. Through this, the efficiency of the multipole excitation (higher multipoles have higher resonant frequencies), and therefore the overall momentum transfer, depend on the impact parameter.

For a small ($r = 1$ nm) particle, for all the excited plasmonic resonances, the longitudinal component of the force is pointed along the beam direction. The direction of the transverse force, though, exhibits more interesting behavior. If the frequency component of the fast electron electromagnetic field is below the multipole resonant frequency, then this multipole's impact is attractive (the excited multipole is "in phase" with the source field). On the other hand, if the frequency component is above the resonance, this multipole's impact is repulsive (the multipole is "out of phase") ([Figure 3.6](#)). For bigger impact parameters, and therefore dominating low frequency components in the Fourier spectrum of the source electromagnetic field, the following is true:

1. The excited dipole resonance prevails over higher-frequency multipole resonances.
2. The frequency components of the source field are far below the dipole resonant frequency. This results in the "dipole in phase" situation and the attractive transverse force.

For smaller impact parameters (< 5 nm), the repulsive force frequency components become dominant, resulting in a repulsive total transverse force

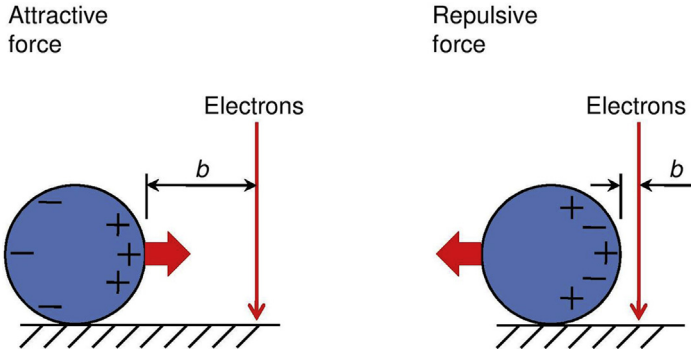


Figure 3.6 Schematic illustration of an electromagnetic force exerted on a particle by a fast-passing electron. The force can be attractive or repulsive, depending on the impact parameter b (following [Batson et al., 2011](#)). (See the color plate.)

exerted on the particle by the beam, which explains the behavior observed in [García de Abajo \(2004\)](#). This phenomenon is due to both the multipolar nature of excitation and the retardation effects.

For small impact parameters, these effects are even more pronounced for larger ($r = 40$ nm) particles, where the higher-order plasmonic multipoles are excited more efficiently and the retardation effects are more pronounced. This results in a much larger repulsive force (bigger than a possible attractive one at larger impact parameters), and even in substantial anti-pushing longitudinal frequency components, the total longitudinal force still remains along the direction of the beam, but it does not rise monotonically. Rather, it starts to decrease for ~ 1 -nm impact parameters. Compared with the $r = 10$ nm particle, the longitudinal component of the force is larger by one to three orders (depending in the impact parameter), while the transverse component is larger by about one order. Finally, the interaction of the beam with a gold nanoparticle with tabulated frequency dependence of the dielectric constant was considered and found significantly different from the one given by the Drude model; this was due to interband transition contributions. It was determined that the force exerted on the particle in this case is defined by high (> 10 eV) frequency tails of the total electromagnetic field, so in this case, it is more proper to speak about the dielectric rather than the plasmonic nature of the force. At the same time, it was noted that the qualitative dependence of the force's spectral components on the impact parameter remain the same as in the plasmonic case, its value becoming approximately one to two orders of magnitude larger.

Now, let us try to estimate the order of the electromagnetic force produced by a single electron using a very simple approach. The transverse component of the electric field produced by a relativistic electron at distance r is given by

$$E = \frac{1}{4\pi\epsilon_0} \frac{e}{r^2} \frac{1}{\sqrt{1 - \left(\frac{v}{c}\right)^2}}. \quad (6)$$

This electric field induces polarization of the particle; thus, the force acting on the particle is obtained as

$$\mathbf{F} = \int \mathbf{P} \cdot \nabla \mathbf{E} \cdot dV. \quad (7)$$

For the case of a spherical particle with radius R and relative permittivity ϵ , we can estimate this force as

$$F = 4\pi R^3 \epsilon_0 \frac{\epsilon - 1}{\epsilon + 2} \cdot E \cdot \nabla E. \quad (8)$$

The calculated electromagnetic force for the case of electron velocity $v/c = 0.7$ and particle relative permittivity $\epsilon = 3$, plotted against the particle radius, was shown previously in [Figure 3.2](#). Separation between the electron trajectory and the particle (impact parameter) is considered to be equal to the radius of the particle.

One can notice that the electromagnetic force produced by a single passing electron is very small and can hardly be stronger than the van der Waals adhesion force, even for particles that are only a few nanometers in size. Thus, a passing electron with its field cannot tear off a particle from a substrate. It can only induce the dragging of a very small cluster over a surface or the motion of bigger particles in a liquid environment (see the section “Electromagnetic Manipulation,” later in this chapter). Let us also estimate momentum transfer induced by a passing electron and time-averaged force produced by an electron beam using Eqs. (6)–(8). For instance, for the case of a particle with $R = 10$ nm and an electron traveling at $v/c = 0.7$ at the distance of 10 nm from the particle surface, we calculate the peak force as $F \approx 0.15$ pN. So the momentum transfer is estimated as $p \approx 8 \times 10^{-30}$ N s ($p \approx F \times \tau$, where $\tau \approx 50 \times 10^{-18}$ s is the dwell time of an electron near the particle). The time-averaged force induced by a 1-nA electron beam (to cite one example) would be $F_{av} \approx 5 \times 10^{-20}$ N ($F_{av} \approx p/t$, where $t = 0.16$ ns is an average time interval between neighboring electrons in the beam).

We would like to note that our estimated value of momentum transfer has the same order as the exact value obtained by [García de Abajo \(2004\)](#) for Al_2O_3 particles of the same size and passing electrons of the same parameters.



3. MECHANICAL MANIPULATION

3.1 Introduction

Mechanical manipulation of microobjects and nanoobjects relies on the usage of various micromanipulators with attached needle-shaped probe tips or microgrippers. All these devices are either commercial or self-made. This manipulation technique is usually based on the mechanical pushing of an object with a probe tip. Pick-and-place manipulation is also possible, either using a microgripper or a single probe tip but involving adhesion mechanisms ([Figure 3.7](#)).

The first work that describes the concept and implementation of a manipulation system installed in an electron microscope chamber was published by [Hatamura and Morishita \(1990\)](#). According to their concept, an operator monitors the process on a magnified three-dimensional (3-D) image from a stereo SEM and manipulates two nanorobots in the vacuum chamber via a bilateral joystick mechanism. They reported that using this system, the operator was able to control the position of micrometer-sized objects with an accuracy of 10 nm. A prototype of a three-axis nanorobot manipulator was developed and installed in a chamber of a stereo SEM that was equipped with a specimen stage that can move along one horizontal axis. A three-axis nanorobot was based on piezoelectric actuators, while the system was additionally equipped with a single-axis force sensor.

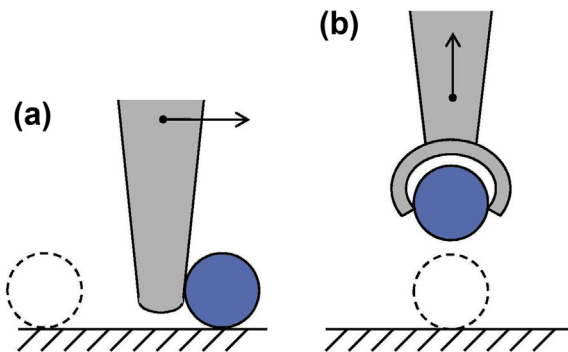


Figure 3.7 Schematic illustration of the mechanical pushing of an object with (a) a needle-shaped probe tip and (b) pick-and-place manipulation using a microgripper. (See the color plate.)

Hatamura and Morishita (1990) tested this prototype by making submicrometer scratches on an aluminium substrate. Miyazaki and Sato (1996) performed the first research on manipulation of microobjects in an SEM. The implemented technique was based on the use of a special micromanipulator with a nominal accuracy of 10 nm installed in the specimen chamber. Using this instrument, polymer microspheres were assembled in ordered structures on a substrate by pick-and-place manipulation using a needle-shaped probe tip and employing adhesion via van der Waals forces.

Modern micromanipulation systems for SEM/TEM are described by Fukuda, Arai, and Nakajima (2013) and references therein. Therefore, this section of this chapter is mainly dedicated to applying micromanipulation systems for handling microobjects and nanoobjects and investigating their mechanical properties. In addition, the principles and characteristics of systems are described briefly.

Some basic principles of modern manipulation techniques in SEMs were reviewed by Jasper (2011). The main part of a micromanipulator is an actuator that should be able to move with nanoscale accuracy. In order to implement such precise movements, the actuator exploits some physical effects. In particular, actuators can be piezoelectric, electrostatic, thermal, or magnetostrictive. Piezoelectric actuators, which are based on the reverse piezoelectric effect, are the most common.

Piezoelectric actuators allow smooth and precise motion. However, their working range is very limited, normally being just a few micrometers. In order to perform coarse positioning in wide range accompanied by fine positioning in short range, a stick-slip principle can be employed based on the inertia and friction. As illustrated in Figure 3.8, a moving part is connected to a fixed piezoelectric actuator using a friction contact. Thus, in the case of slow deformation of the actuator, the moving part follows it (the stick phase). In the case of abrupt contraction of the actuator, the moving part slips and does not move (the slip phase). The sequence, consisting of alternating stick and slip motion phases, provides coarse positioning over a wide range, while the stick phase itself provides fine positioning over a short range.

3.2 Commercial Micromanipulators

Micromanipulators for electron microscopes are produced by several companies. The leading manufacturers include Kleindiek Nanotechnik (based in Reutlingen, Germany), Klocke Nanotechnik (Aachen, Germany), Oxford Instruments (Abingdon, England), Zyvex Instruments (Richardson, Texas), SmarAct (Oldenburg, Germany), FEI (Hillsboro, Oregon), Imina

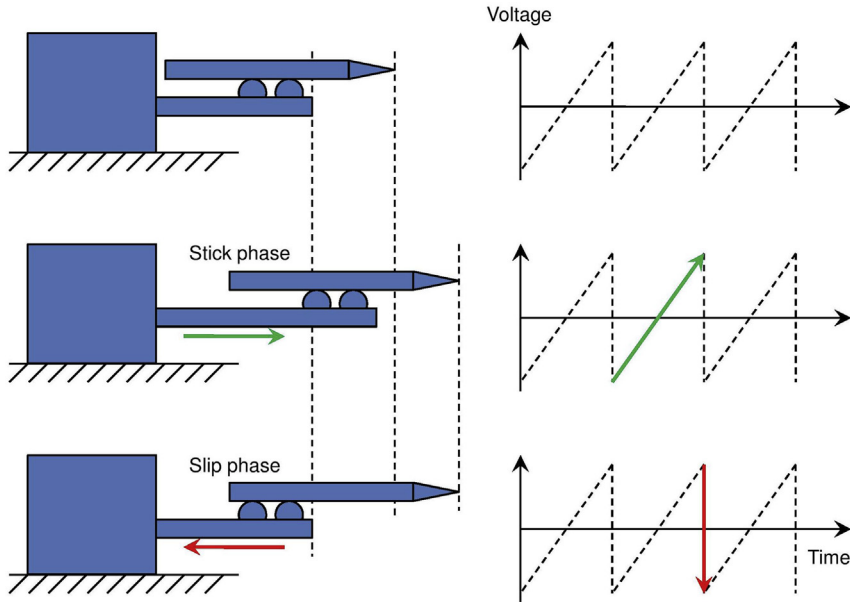


Figure 3.8 The stick-slip principle of motion of piezoelectric actuators. (See the color plate.)

Technologies (Lausanne, Switzerland), Hummingbird Scientific (Lacey, Washington), and Xidex (Austin, Texas).

These manipulators differ in dimensions; some of them are compact and can be mounted inside the SEM chamber on a wall or on a translation stage, while others have to be port-mounted on the wall of the chamber partly outside. Also, a micromanipulator made by Imina Technologies is a mobile robot called miBot, while Hummingbird Scientific offers a special holder for manipulation in TEMs. All manipulators have low vibration constructions to achieve high resolution, low backlash, and drift.

In all these micromanipulators, the piezoelectric effect is employed for at least fine motion. Coarse motion is achieved either by the stick-slip principle or a separate motorized control. Almost all manipulators have a Cartesian coordinate system, but a polar coordinate system and a combination of the Cartesian and the polar systems are also used. A micromanipulator OmniProbe from Oxford Instruments provides the Cartesian system with additional rotational motion. Also, the possibility of multiple degrees of freedom is provided by SL-line and SR-line micromanipulators from SmarAct.

The described micromanipulators provide precision of motion ranging from a few nanometers down to subnanometers. Some micromanipulators

have a position sensor that provides a feedback loop. Micromanipulators can also be equipped with various optional tools, such as microgrippers and force sensors. Special probe tips suitable for mechanical and electrical characterization also can be installed. Micromanipulators are able to achieve significant forces, which are sufficient for handling any kind of microobjects and nanoobjects. For instance, an MM3A-EM micromanipulator from Kleindiek Nanotechnik provides a holding force of 1 N, whereas the gripping force ranges from 5 to 5000 μN . The main characteristics of the reviewed micromanipulators are summarized in Table 3.1.

3.3 Handling Microobjects and Nanoobjects and Investigation of Their Mechanical Properties

A standard application of manipulators in electron microscopy (particularly, in dual electron-ion beam workstations) is the fabrication of TEM lamellae. The basic procedure of the fabrication and some of its features are described in various publications (e.g., Mayer *et al.*, 2007). In this procedure, the lamella is cut by focused ion beam milling, whereas manipulation is used to transport a probe tip with a welded lamella to a TEM grid.

More advanced manipulation of microobjects and nanoobjects requires either the usage of modified commercial micromanipulators or developing self-made manipulators. For instance, Peng *et al.* (2004) demonstrated the gripping of nanoobjects using a manipulation system comprised from four Kleindiek Nanotechnik nanoprobes installed in an SEM. A number of studies are dedicated to the manipulation and characterization of carbon nanotubes in SEMs using manipulation systems with multiple degrees of freedom. For example, Yu *et al.* (1999) developed a piezomanipulator with XYZ translation and one rotational motion, whereas Fukuda *et al.* (2003) constructed a nanorobotic manipulator with 16 degrees of freedom. Hänel *et al.* (2006) used a scanning tunneling microscope integrated in an SEM for the manipulation of organic nanocrystallites. Zhang *et al.* (2013) developed a nanomanipulation system that can be installed in the SEM chamber via a load-lock. Micromanipulators also can be used in TEMs, although the space there is limited. For instance, Dong *et al.* (2008) developed a system that is integrated into a TEM holder.

Micromanipulators can use not only needle-shaped probe tips, but also microgrippers. The gripping mechanism can be based on physical effects of varying types, such as piezoelectric (Clévy *et al.*, 2005), electrostatic (Mølhave *et al.*, 2006), electrothermal (Cagliani *et al.*, 2010), or a shape memory effect (Nakazato *et al.*, 2009). The most advanced microgripper,

Table 3.1 Main Characteristics of Commercial Micromanipulators

Manufacturer	Mounting	Motion Principle	Coordinate System	Motion Precision	Optional Tools
Kleindiek Nanotechnik (www.nanotechnik.com)	Inside the SEM chamber	Piezo, stick-slip; holding force: 1 N	Polar + optional rotation	0.5–5 nm	Microgripper (gripping force: 5–5000 μ N), rotational tip, force sensor, electrical characterization
Klocke Nanotechnik (www.nanomotor.de)	Inside SEM chamber	Piezo	Cartesian	1 nm	Position sensor, force sensor
Oxford Instruments (www.oxford-instruments.com/)	Flange-mounted, partly outside SEM	Piezo	Cartesian and optional rotation	Sub-nm, 10 nm in feedback loop	Position sensor, electrical characterization
Zyvex (www.zyvex.com)	Inside SEM chamber	-	Cartesian	5 nm	
SmarAct (www.smaract.de)	Inside SEM chamber	Piezo, stick-slip	Cartesian, optional multiple degrees of freedom	Sub-nm, 1 nm in feedback loop	Microgripper
Imina Technologies (www.imina.ch)	Mobile	Piezo	Cartesian and polar	0.5 nm	Microgripper, optical fiber
Hummingbird Scientific (hummingbirdscientific.com)	TEM mounted	Fine piezo and motorized coarse	Cartesian	1 nm	N/A
Xidex (www.xidex.com/)	Inside SEM chamber	Piezo, stick-slip	Cartesian	Sub-nm	Microgripper, force sensor

which was tested by [Cagliani *et al.* \(2010\)](#), was able to handle nanowires and nanotubes of sub-100-nm diameters.

This material has described mechanical micromanipulations in electron microscopes performed manually when an operator controls the movement, monitoring it via SEM/TEM images. However, presently this process can be done automatically, with the system performing all the manipulations itself via vision-based motion control. Such automatic manipulation is faster, and it does not depend on the operator's skills. The first automatic manipulation system for an SEM was constructed by [Kasaya *et al.* \(2004\)](#), who demonstrated pick-and-place manipulation of 30- μm metal spheres. The motion of the probe tip relied on an image recognition system that used filtered SEM images to detect edge fragments. Moreover, a force sensor gave information about this event. Pickup of a sphere by a probe tip occurred via the adhesion mechanism (further investigation of adhesion in SEMs performed by the same group is described later in this chapter). Some newer research on this topic ([Eichhorn *et al.*, 2009](#)) describes the use of a microgripper in the automatic mode for handling carbon nanotubes. Other studies by the same scientists ([Jasper & Fatikow, 2010](#); [Jasper, 2011](#)) also investigated ways of overcoming a natural limitation of an SEM, which reduces the speed of manipulations: according to these findings, scanned images of a moving object obtained in an SEM give a distorted picture. Increasing the scanning speed reduces the distortion but causes noisy, poor-quality images. A possible solution, which allows tracking the object fast and precisely, is a technique involving two line scans, which is schematically illustrated in [Figure 3.9](#).

A number of other studies have been dedicated to the visual tracking of motion in an automatic mode, and they have looked at techniques such as improving electron image processing using contour models ([Ru *et al.*, 2012a](#)) or contact detection purely based on image recognition ([Ru & To,](#)

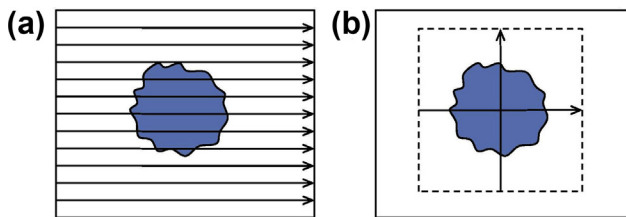


Figure 3.9 Schematic illustration of tracking of an object by (a) normal SEM imaging and (b) a two-line scan. The latter is more suitable for automatic tracking. (See the color plate.)

2012b). Visual contact detection was also employed by Zhang *et al.* (2012) during the fabrication of nanowire-based field-effect transistors. The research performed by Ye *et al.* (2013) is dedicated to three-dimensional (3-D) automatic navigation, which is needed to pick up a freestanding nanowire with a probe tip [see also Ye (2012) and references therein].

Another classical application of micromanipulators is providing contacts to local positions on the surface of microobjects and nanoobjects, which are mostly one-dimensional (1-D) structures (e.g., nanowires, nanotubes, and nanobelts) to investigate their electrical characteristics (the electron beam is usually blanked for the time of the measurement). While this technique does not require any manipulation with objects, there are studies where manipulation ability has been employed. Manipulation can be used for either mechanical deformation of the object in order to study dependence of electrical characteristics on the deformation, or for assembling of objects in order to study characteristics of complex structures. For instance, Kim *et al.* (2003) studied electrical characteristics of multiwall carbon nanotubes in an SEM, equipped with two micromanipulators with tungsten probe tips. In particular, the authors investigated the field emission properties of a single nanotube. The nanotube was welded to a tip of the first manipulator, whereas the second manipulator was positioned a few micrometers from a freestanding end of the nanotube. Another section of the same paper was dedicated to studying the current-voltage characteristics of the nanotube bent between two tips of the micromanipulators. Bussolotti *et al.* (2007) also investigated the electrical characteristics of multiwall nanotubes with the help of micromanipulators. The nanotubes were grown on a nickel surface; the approaching tip of a micromanipulator was welded to a freestanding end of the nanotube to provide an electrical contact. Measurements of current-voltage characteristics showed that the electrical resistance of the nanotube increases several orders of magnitude upon bending the tube from a straight shape to a U-shape. Liu *et al.* (2008) investigated the current-voltage characteristics of a bent ZnO nanowire. The experiment was performed in a TEM equipped with a special specimen holder with a piezomanipulator. Using the high-resolution TEM technique helped to determine a crystalline structure of the bent nanowire, which was linked to its electrical properties (Figure 3.10). Also, a recent study by Mai *et al.* (2012) is dedicated to the mechanical and electrical characterization of ZnO nanorings. The authors studied not only the current-voltage characteristics of a nanoring, but also its mechanical properties, by compressing an individual nanoring with

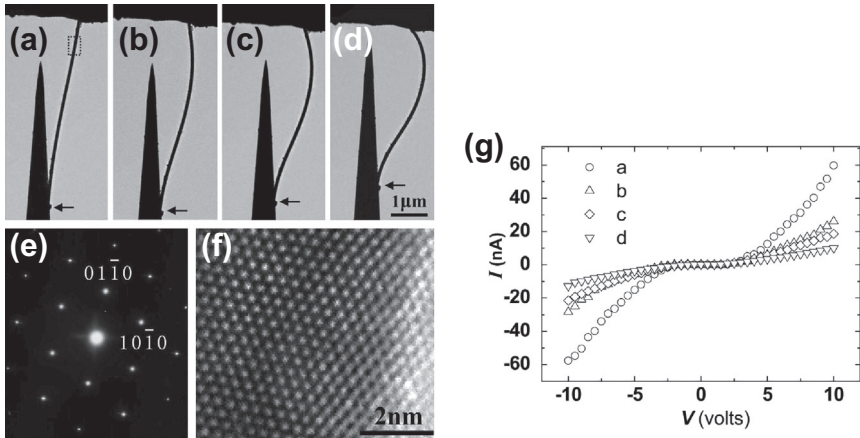


Figure 3.10 Measurement of current-voltage characteristics of a ZnO nanowire upon its bending using a piezomanipulator integrated into a specimen holder of a TEM. Reproduced with permission from Liu *et al.* (2008). Copyright by AIP Publishing LLC.

two micromanipulators in an SEM. Other research related to mechanical characterization is reviewed in detail next.

Investigation of various mechanical properties of microobjects and nanoobjects (e.g., adhesion, hardness, and friction) is another application of micromanipulators in electron microscopes. Most of the research in the field of quantitative nanomechanics was performed with the help of atomic force microscopy (e.g. Götzinger & Peukert, 2003). But only a micromanipulator with a force sensor installed in an electron microscope provides a unique capability of measurement and real-time visualization of the process. However, as already noted, an electron beam charges objects, which can greatly affect the measurements. Nevertheless, the analysis of the experimental results obtained at these conditions provides a guideline for reliable micromanipulation, particularly in automatic mode.

For instance, some experimental aspects of adhesion of polymer micrometer-sized spheres under electron beam illumination were investigated by Miyazaki *et al.* (2000a, b), who developed a special adhesion force measurement system installed in an SEM. This system was based on a movable metalized probe tip and a substrate with laser interferometer to detect the displacement. This allowed the measurement of an adhesion force of micrometer-sized polymer particles deposited on a gold substrate. The obtained value for adhesion ranged from 50 to 3000 nN. In particular, the authors observed an increase of the adhesion force with the time spent

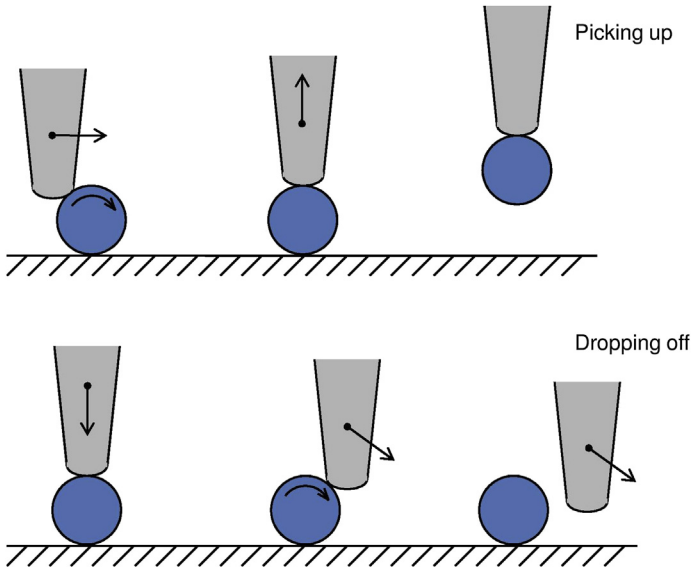


Figure 3.11 Schematic illustration of a pick-and-place manipulation strategy based on an adhesion effect (following [Saito et al., 2002](#)). (See the color plate.)

on electron beam illumination, which was attributed to charging and an electrostatic contribution to adhesion. Some further experiments on adhesion measurement and adhesion-based manipulation were performed by [Saito et al. \(2002\)](#) using a needle-shaped probe tip in an SEM. Here, the kinematics of the rolling and slipping motion of microspheres was investigated both theoretically and experimentally. As a result, a reliable method of pick-and-place operations was proposed (as shown in [Figure 3.11](#)).

Mechanical micromanipulation also can be employed to investigate the hardness of nanoobjects. For instance, [Enomoto et al. \(2006\)](#) experimentally measured Young's modulus of carbon nanotubes fabricated using different methods: arc discharge, catalytic chemical vapor deposition, and thermal chemical vapor deposition. The apparatus for Young's modulus measurement was installed in a TEM and consisted from a stationary stage with a specimen and an XYZ piezodriving stage with an atomic force microscope cantilever attached. The measurement principle was based on bending the nanotube upon an applied force ([Figure 3.12](#)). Moreover, TEM operating at 200 kV enabled the visualization of a crystalline structure of the nanotube. The authors demonstrated that nanotubes obtained by arc discharge have the highest crystallinity, and their measured Young's modulus of 3.3 TPa is very close to the theoretical value. [Nakajima, Arai, and Fukuda \(2006\)](#) developed

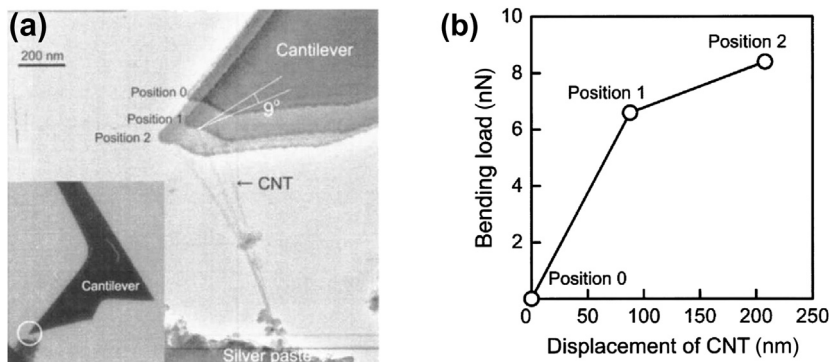


Figure 3.12 Experimental investigation of the Young's modulus of a carbon nanotube using a special apparatus installed in a TEM. *Reproduced with permission from Enomoto et al. (2006). Copyright by AIP Publishing LLC.*

a hybrid manipulation system with multiple degrees of freedom, which can be installed in a TEM or an SEM. A manipulator with 8 degrees of freedom placed inside an SEM performed preliminary positioning. Then a small unit with 3 degrees of freedom could be fitted in a limited volume of a TEM for final manipulation with a higher precision. To demonstrate the effectiveness of the system, the measurement of the Young's modulus of carbon nanotubes was performed. Investigation of mechanical properties of another one-dimensional nanostructure, a silver nanowire, was performed by Vlassov et al. (2014). The experiments were conducted inside an SEM equipped with a self-made force sensor. The Young's modulus and yield strength were found to be 90 GPa and 4.8 GPa, respectively. Notably, no dependence on the nanowire diameter was observed. High fatigue resistance of silver nanowires was also demonstrated.

Measurement of friction at the nanoscale can also be done with the help of mechanical micromanipulation in electron microscopes. A series of recent experiments (Vlassov et al., 2011; Polyakov et al., 2011, 2012, 2014) presents results of investigations of the tribological properties of various nanoobjects. For these experiments, a micromanipulation system was developed and installed in an SEM. The system consisted of an atomic force microscope cantilever glued to a quartz tuning fork force sensor. The authors studied the static friction of 150-nm gold nanoparticles and found it to be in the range of 40–750 nN. ZnO nanowires were another object of investigation, where translation of a nanowire over a surface and the resulting elastic deformations were used to determine a distributed friction force. Also, the

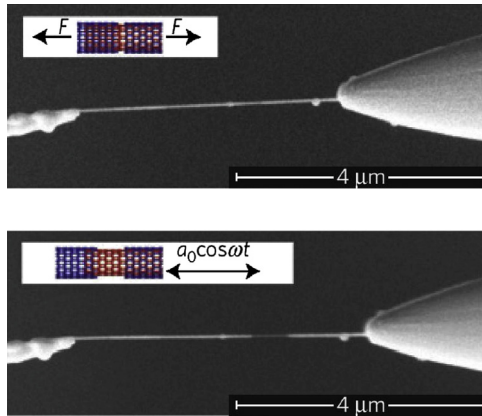


Figure 3.13 Experimental investigation of interlayer friction in a boron nitride nanotube performed in an SEM. *Reproduced with permission from Niguès et al. (2014). Copyright by Nature Publishing Group. (See the color plate.)*

dependence of static friction of CuO nanowires on the surface roughness was investigated. The experimental results suggest a considerably smaller friction force for smoother surfaces; this differs from the macroscale situation, where friction has no dependence on the contact area. The same group carried out another study that looked at the tribological properties of silver nanodumbbells. These objects are characterized by reduced contact area and adhesion in comparison to nanowires. Different types of nanodumbbell motion (i.e., rolling, sliding, and rotation) were demonstrated. Another interesting investigation of the friction of nanomaterials was performed by Niguès et al. (2014). They studied interlayer friction in a boron nitride nanotube using an SEM and used a quartz tuning fork as a force sensor. A nanotube was torn apart, and the measured friction was found to be proportional to the contact area (see Figure 3.13).

4. ELECTROSTATIC MANIPULATION

The electrostatic manipulation technique is based on the electrostatic interaction between objects charged under electron beam illumination. Random motion or deformation of the specimen objects due to charging is an unwanted effect, which sometimes can be observed in an electron microscope. This includes for example, the accidental shifting of dielectric particles during SEM imaging or tearing a thin film in the case of a TEM. However, the effect of specimen charging can also be employed to produce controllable motion (i.e., manipulation).

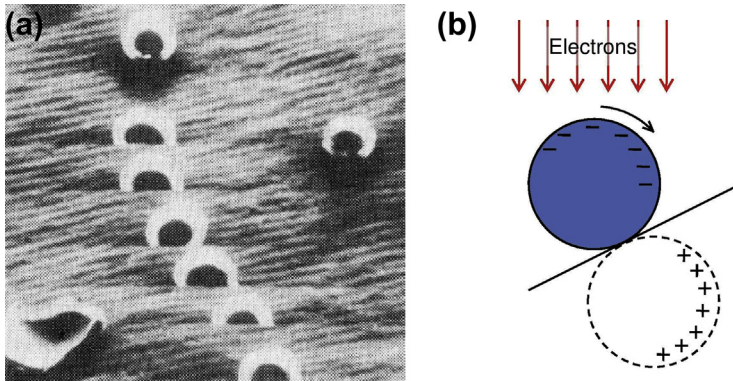


Figure 3.14 (a) Rolling motion of a spherical polystyrene particle observed on a single SEM image with a 40-s recording rate. Reproduced with permission from [Krakow and Nixon \(1977\)](#). Copyright by IEEE. (b) Schematic illustration of an uphill motion mechanism that occurs due to a torque that is produced by an attractive force between particle charge and its mirror image in a substrate when the latter is tilted (following [Krakow & Nixon, 1977](#)). (See the color plate.)

One of the first works related to this topic was published by [Krakow and Nixon \(1977\)](#). The authors studied charging phenomenon during SEM imaging of 10- μm polystyrene and glass spherical particles mounted on a gold-coated grating substrate. Total charge accumulated by a particle was found to be 10^{-12} C, which was estimated from the distortion of the SEM image. When the substrate was tilted more than 17° , directed rolling motion of particles was observed ([Figure 3.14a](#)). Moreover, when a low-energy electron beam (10 kV) was applied, the spherical particles rolled uphill, whereas downhill motion was observed at higher electron energies (i.e., 20 kV). This effect occurred due to the torque produced by an attractive force between the negative charge in the particle and an induced mirror charge in the conductive substrate. This explains the uphill motion at 10 kV that is illustrated in [Figure 3.14b](#). Downhill motion at 20 kV is believed to be due to deeper localization of the negative charge within the particle. As a result, the torque appeared to be the opposite. Krakow and Nixon also performed a theoretical study of the effect to investigate the qualitative dependence of the torque and velocity of a sphere rolling, as opposed to the substrate tilt angle.

Another study is dedicated to the controllable deflection of Si nanowires in response to electron beam illumination ([Fukata et al., 2005](#)). The authors observed motion while imaging a pair of nanowires grown on a Si wafer. They found that the separation between the nanowires increases upon the

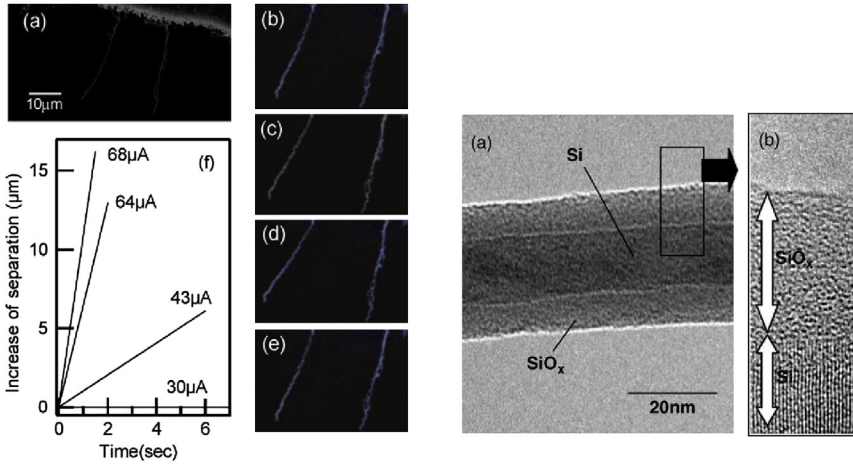


Figure 3.15 SEM images showing controllable deflection of Si nanowires due to their charging under electron beam illumination. The increase of separation between the nanowires is plotted against the time of illumination for different electron beam currents. (left). TEM images confirm the structure of a Si nanowire with a SiO_x surface layer, which is responsible for charge accumulation (right). *Reproduced with permission from Fukata et al. (2005). Copyright by IOP Publishing. (See the color plate.)*

increase of the electron beam current and imaging time (Figure 3.15). After electron beam illumination finishes, the distance between the nanowires returns to the initial value immediately. The authors suggest that the motion was caused by the Coulomb repulsive interaction between the nanowires. The charge is believed to be accumulated in a SiO_x surface layer, which covers the Si crystalline core of the nanowire. The conductive Si core is also responsible for the fast discharge after the completion of electron beam illumination.

Charge patterns created on a dielectric substrate in an SEM can be used for nanoparticle assembly, as demonstrated by Zonnevylle *et al.* (2009). Positively charged Pd nanoparticles were created in an Ar atmosphere from a glowing wire generator in a deposition chamber. Gas flow with suspended nanoparticles passes through a differential mobility analyzer for the selection of particles of a certain size and charge. At the same time, in an SEM chamber, Si substrate with a 6-μm-thick layer of Si₃N₄ was exposed by a 6-kV electron beam in order to create an array of negative charges. The substrate was then transferred from the SEM chamber to a deposition chamber, where particles were deposited from the gaseous suspension and assembled on charged places of the substrate (Figure 3.16).

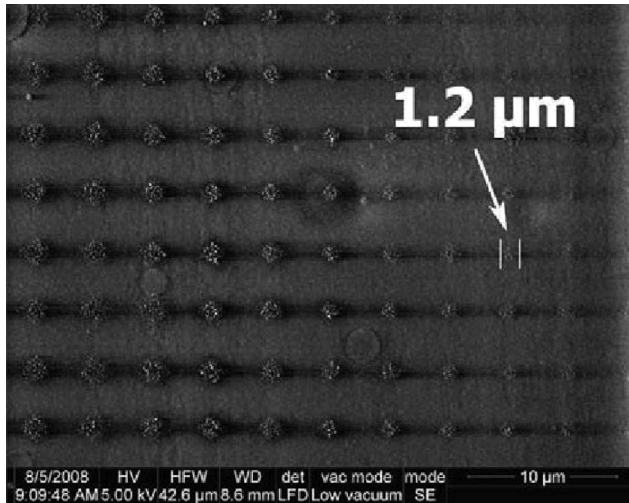


Figure 3.16 Positively charged Pd nanoparticles from gaseous suspension assembled on a negative charge pattern created by an electron beam on a Si_3N_4 -coated Si substrate. Reproduced with permission from [Zonneville et al. \(2009\)](#). Copyright by Elsevier.

Pick-and-place manipulation of microparticles and nanoparticles can be performed using a needle-shaped probe tip and employing various electrostatic effects caused by charging under electron beam illumination. For instance, [Ampem-Lassen et al. \(2009\)](#) created a single photon source by such manipulation of a 300-nm diamond nanocrystal in an SEM. The authors used a micromanipulator with a carbon-coated, tapered optical fiber tip attached. When the tip of the micromanipulator approached the diamond nanocrystal sitting on a substrate, the nanocrystal favored the tip (sometimes even jumping from the substrate onto the tip) and could be transported. This pickup effect is believed to be due to the electrostatic interaction resulting from charging in the SEM; however, the exact mechanism was not well explained. [Denisyuk et al. \(2012\)](#) and [Denisyuk, Komissarenko, & Mukhin \(2014\)](#) performed some further investigation of this manipulation technique. In particular, [Denisyuk, Komissarenko, & Mukhin \(2014\)](#) reported about pick-and-place manipulation of Al_2O_3 , WO_3 , and tungsten microparticles and nanoparticles of various shapes ([Figure 3.17](#)). This experiment was performed in an SEM employing a nongrounded metalized tip glued to a micromanipulator. The authors demonstrated a well-controlled pickup and drop-off of the particles by the tip. Moreover, the drop-off was demonstrated in two ways: shifting the electron beam from the metallic tip and pulling the tip aside.

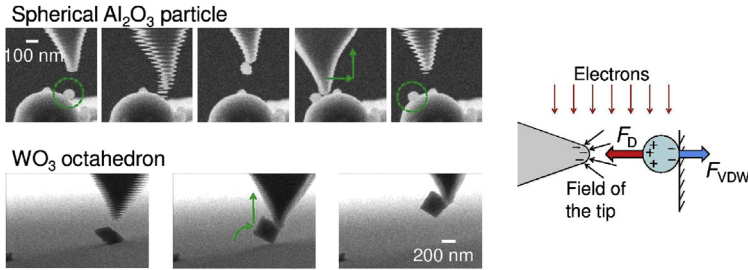


Figure 3.17 Pick-and-place manipulation of an 80-nm Al_2O_3 spherical particle and a WO_3 nanooctahedron in an SEM. The schematic on the right illustrates the mechanism: A particle is retained on a substrate by the van der Waals force, while a nongrounded metallic tip charged under electron beam illumination creates a dielectrophoretic force that pulls the particle from the substrate to the tip. *Reproduced with permission from Denisyuk, Komissarenko, & Mukhin (2014). Copyright by Elsevier. (See the color plate.)*

Denisyuk, Komissarenko, & Mukhin (2014) also created a theoretical model to explain the pickup effect. This model was based on the assumption that particles are retained on the substrate by the van der Waals force, whereas a nongrounded metallic tip gets charged under electron beam illumination and creates electrostatic field gradient and dielectrophoretic forces, which pulls the particle from the substrate to the tip (Figure 3.18). The dielectrophoretic force was computed as an integral over the particle volume:

$$\mathbf{F} = \int (\mathbf{D} - \epsilon_0 \mathbf{E}) \nabla \mathbf{E} dV, \quad (9)$$

where \mathbf{E} is the local electric field and \mathbf{D} is the local electric displacement field. The tip was supposed to be charged up to the maximum possible value, which was limited by the field emission effect.

Electrostatic manipulation due to the charging effects can be achieved in a TEM as well. However, two cases, discussed next, cannot be considered to be controlled manipulation, but rather, an observed phenomenon of nanoparticle motion induced by some electrostatic mechanism. For example, White *et al.* (2012) studied the dynamics of nanoparticles in a liquid environment. In this experiment, 4-nm Pt nanoparticles were deposited on an insulating membrane of an electron-transparent cell filled with deionized water (Figure 3.19). During imaging the area of $350 \times 350 \text{ nm}^2$ at 300 kV, it appeared that initially immobile particles started to move away from the exposed area. Particle trajectories were directed radially outward from the center, and the dispersion rate increased as the electron beam current

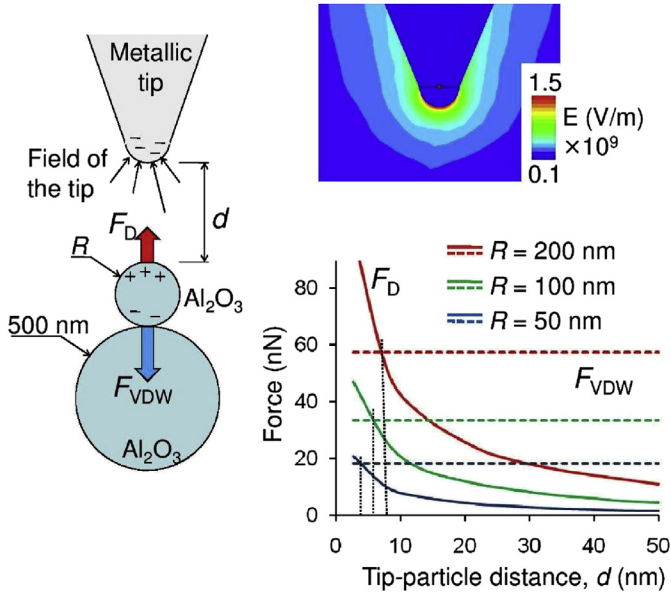


Figure 3.18 Theoretical model of a particle pickup effect: A schematic illustration, distribution of the electric field around the charged tip, and a chart that shows the calculated van der Waals holding force and dielectrophoretic pulling force. *Reproduced with permission from Denisjuk, Komissarenko, & Mukhin (2014). Copyright by Elsevier. (See the color plate.)*

increased from 5 to 57 pA. The observed effect of radially directed motion of the nanoparticles was attributed to the electrophoresis caused by the charging of the membrane and the nanoparticles. [White *et al.* \(2012\)](#) repeated this experiment with a dry sample in a high-vacuum environment under the same imaging conditions, but no motion was detected. Thus, the presence of water reduced the adhesion between the particles and the membrane and allowed the movement of the particles.

The other example of electrostatic motion was observed by [Xu *et al.* \(2010\)](#) in a TEM with normal dry conditions. The authors deposited CdSe nanocrystals on a carbon film from a toluene solution. While imaging of a dried specimen at 200 kV took place, a remarkable effect was detected: one of the thousands of CdSe nanocrystals did not sit on the film; rather, it levitated and slowly rotated ([Figure 3.20](#)). The authors suggest that this single 10-nm nanocrystal was trapped in a 3-D Coulomb potential well that was formed due to the charge of the nanocrystal and a unique distribution of two charged rings on the carbon film in a thin-insulating layer that was accidentally deposited with the nanocrystals from the solution

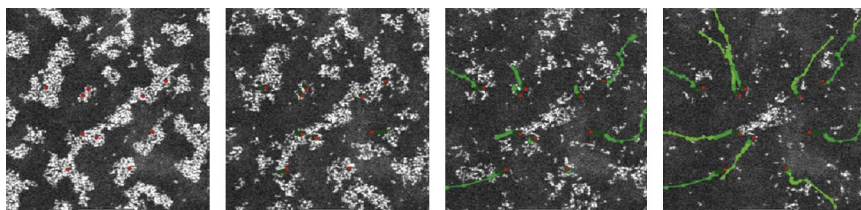


Figure 3.19 Motion of Pt nanoparticles deposited on an insulating membrane of a liquid cell after imaging in a scanning TEM operating at 300 kV with a beam current of 57 pA. The images were taken at 7-s intervals. *Reproduced with permission from White et al. (2012). Copyright by American Chemical Society. (See the color plate.)*

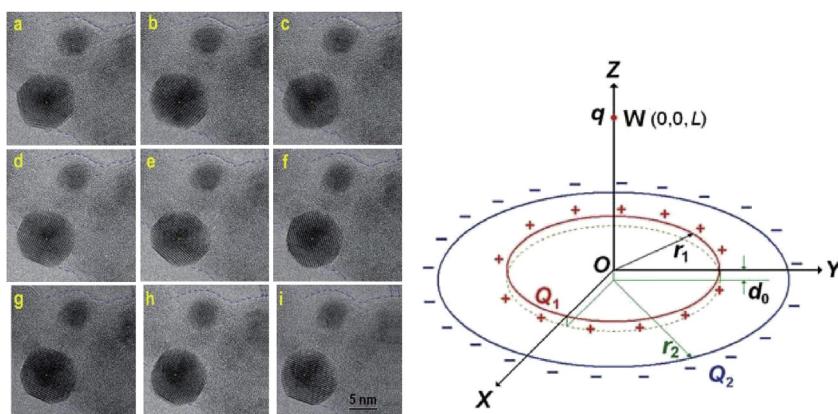


Figure 3.20 A remarkable effect of levitation and slow rotation of a single CdSe nanocrystal over a carbon substrate while imaging in a TEM at 200 kV is shown on the left (the images were captured consequently during 10 minutes of observation). A schematic illustration of the charge distribution, which can cause a 3-D Coulomb potential well responsible for the levitation, is shown at the right. *Reproduced with permission from Xu et al. (2010). Copyright by American Chemical Society. (See the color plate.)*

(Figure 3.20). In this case, the Coulomb potential energy of the nanocrystal is given by

$$U(z) = \frac{q}{4\pi\epsilon_0} \left(\frac{Q_1}{\sqrt{r_1^2 + z^2}} + \frac{Q_2}{\sqrt{r_2^2 + (z + d_0)^2}} \right), \quad (10)$$

and a potential well responsible for the levitation is produced. Xu *et al.* also suggest that the observed rotational motion of the particle was caused by inelastic interaction with the passing electrons and the fact that the shape and crystalline structure of the particle were somewhat asymmetric. The

electromagnetic force caused by passing electrons and its influence on the particle rotation were not considered in this chapter.



5. ELECTROMAGNETIC MANIPULATION

The electromagnetic manipulation technique is based on the influence of the electromagnetic force created by fast electrons. The underlying physics was first considered in the theoretical work by [García de Abajo \(2004\)](#), as described in the section “Electromagnetic Force Exerted on a Particle by Fast-Passing Electrons,” earlier in this chapter. The first experimental confirmation of this effect was obtained by [Oleshko and Howe \(2011\)](#) using a TEM.

Due to the similar nature of the optical trapping of particles in optical (or laser) tweezers, such electromagnetic manipulation is known as *electron trapping* or *electron tweezers*. However, in contrast to optical tweezers, which can manipulate submicrometer-sized or larger particles, electron tweezers can operate much smaller particles (with sizes down to 1 nm). Recent developments and progressive use of aberration-corrected TEMs, providing resolutions down to the subangstrom range, further pushed the experimental investigation of this effect. [Oleshko and Howe \(2013\)](#) reviewed electron tweezers in a great deal of detail. Thus, in this review we will just briefly discuss the main experimental results related to this topic.

[Oleshko and Howe \(2011\)](#) described the manipulation of a crystalline Al nanosphere floating in an Al-Si molten alloy bead observed in a TEM at 197 kV (as shown in [Figure 3.21](#)). The motion occurred with translation of the beam or with moving the microscope stage. Rotation of the particle under electron illumination was also detected. The effects were attributed to the momentum transfer from the fast electrons to the floating Al nanosphere. The authors reported a rather high value for momentum transfer, which was estimated from the detected motion speed of the nanosphere and was found to be in the range of 10^{-27} – 10^{-26} N s. Also, they considered forces exerted on the solid nanoparticle in a liquid environment under electron illumination. The total force is given by

$$\mathbf{F} = \mathbf{F}_d + \mathbf{F}_{gv} + \mathbf{F}_b + \mathbf{F}_r + \mathbf{F}_{gd}, \quad (11)$$

where \mathbf{F}_d is the drag or fluid resistance force, \mathbf{F}_{gv} is the gravitational force, \mathbf{F}_b is the buoyant force, \mathbf{F}_r is the radiation force (due to emitted radiation as a result of the interaction with the electrons), and \mathbf{F}_{gd} is the electromagnetic gradient force induced by the fast electrons. The theoretical value for the electromagnetic force was not provided by [Oleshko and Howe \(2011\)](#).

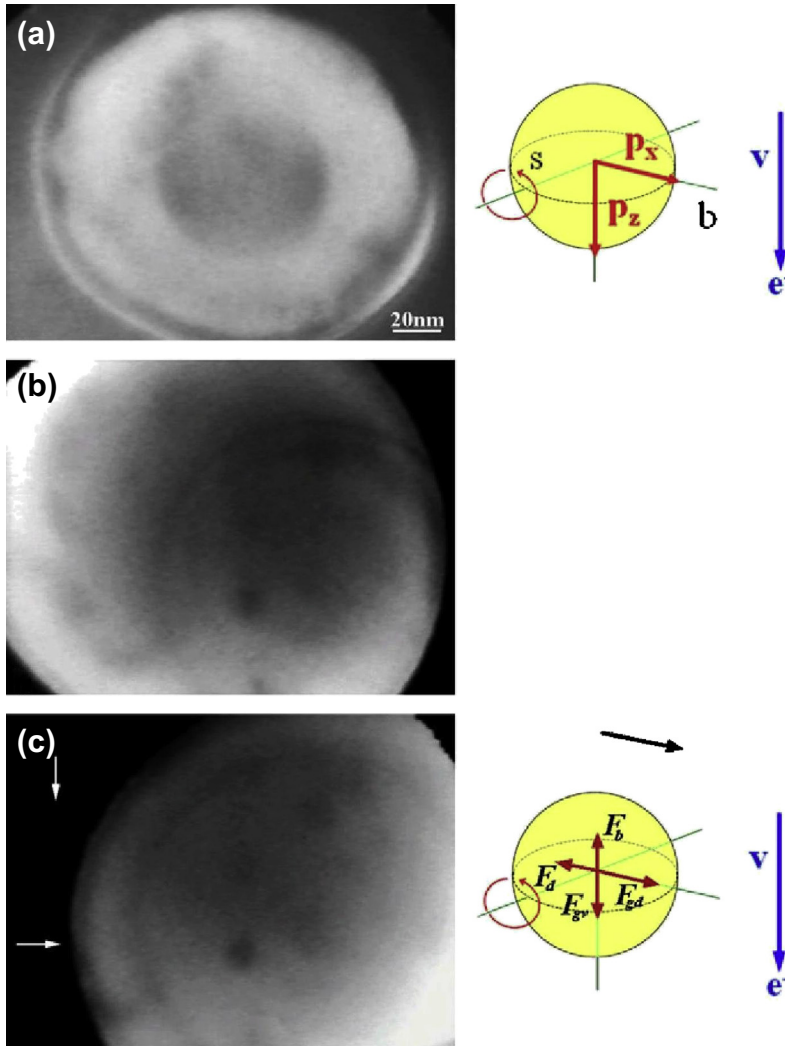


Figure 3.21 TEM image of a 70-nm-diameter crystalline Al nanosphere floating in an Al-Si molten alloy bead (a). Motion of the nanosphere was observed upon translation of the electron beam (b) or upon moving the microscope stage (c). *Reproduced with permission from Oleshko and Howe (2011). Copyright by Elsevier. (See the color plate.)*

Individual nanoparticle manipulation using an electron beam also can be performed in a liquid cell, as reported by Zheng *et al.* (2012). The liquid cell contained a solution with 10-nm gold particles sandwiched between two silicon nitride membranes. For the purpose of manipulation, a 120-kV electron beam was focused on the spot with a Gaussian profile and a diameter

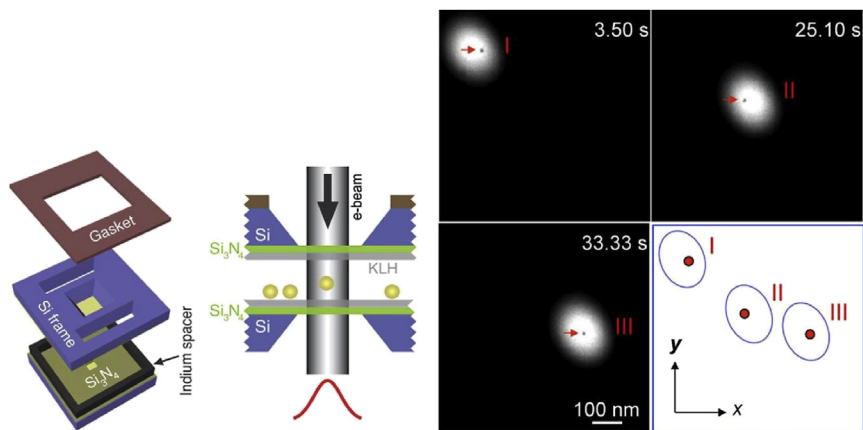


Figure 3.22 Schematic illustration of nanoparticle manipulation inside a liquid cell in a TEM (left), and sequential images demonstrating the motion of an individual gold nanoparticle that follows shifting of the electron beam (right). *Reproduced with permission from Zheng et al. (2012). Copyright by American Chemical Society. (See the color plate.)*

in the range of 50–200 nm. An individual particle was then trapped inside the beam and moved following the beam shift (see Figure 3.22). Some Brownian motion of the nanoparticle within the beam was also observed, but the particle did not escape the focusing spot. The authors also estimated that the trapping force produced by the electron beam should be in the order of piconewtons. At the same time, the mechanism of the trapping was not clearly explained, but the authors did discuss that factors such as negative pressure, charging, and thermophoresis caused by the passing electrons might contribute to the effect, but the electromagnetic force induced by the electron beam was not taken into account.

Electromagnetic manipulation of nanoparticles on a substrate in high-vacuum conditions is also possible; however, it was demonstrated only for particles that are a few nanometers in size. For instance, Batson *et al.* (2011 and 2012) reported experimental results on the controlled motion of gold clusters over a carbon substrate in response to 120-kV electrons. The clusters were imaged in a scanning TEM mode with aberration correction. The electron beam stopped at the beginning of each line at the left edge of the scanned area, producing most of the impact on the cluster. The distance between the left edge of the frame and the cluster, called the *impact parameter*, was crucial to the manipulation process. For instance, in the case of a single 1.5-nm cluster and moderate impact parameters, the electron beam caused an attractive force, and so the cluster moved toward

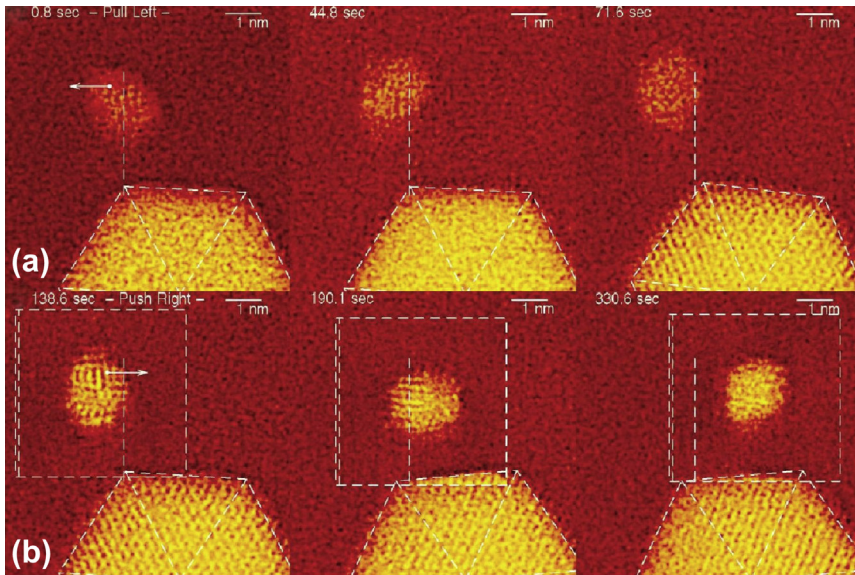


Figure 3.23 Guided motion of a 1.5-nm gold cluster: attractive pulling induced by a moderate impact parameter of 4.5 nm (top), and repulsive pushing resulting from a small impact parameter of 1 nm. *Reproduced with permission from Batson et al. (2011). Copyright by American Chemical Society. (See the color plate.)*

the left edge. On the other hand, for small impact parameters, the force was repulsive and the cluster motion was in the opposite direction (Figure 3.23).

Additional experiments were performed with cluster pairs, where attraction and repulsion between clusters were observed depending on the electron beam placement. The effect of motion was attributed to the influence of an electromagnetic field of the passing electrons, which causes polarization of the particles and induces long-ranged attractive and short-ranged repulsive forces between the electron beam and the particle. The observed effects were explained with the theoretical approach by Reyes-Coronado *et al.* (2010), as discussed in the section “Electromagnetic Force Exerted on a Particle by Fast-Passing Electrons,” earlier in this chapter. The authors also note that some additional effects (e.g., specimen charging and heating) may contribute to the motion of the clusters.

Another experiment about the manipulation of nanoparticles on a substrate was performed by Verbeeck *et al.* (2013). Approximately 3-nm gold particles were sitting on a Si_3N_4 supporting film and imaged in a TEM operating at 300 kV. The TEM was equipped with a holographic mask that

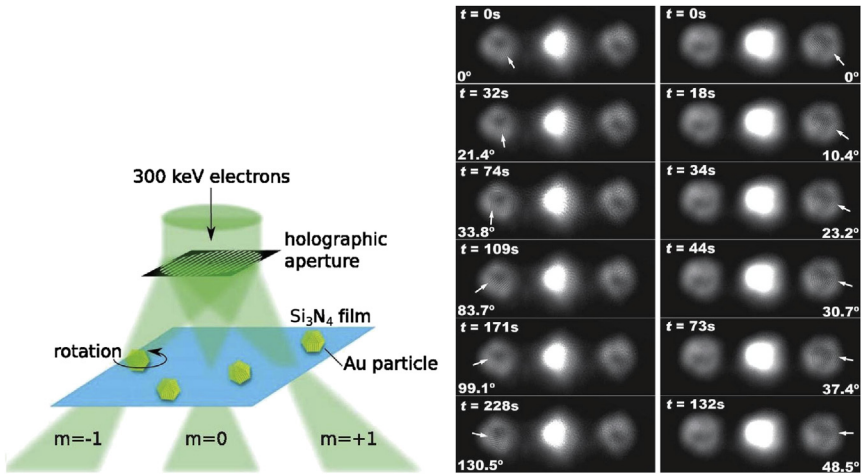


Figure 3.24 Schematic illustration and experimental imaging of particle rotation upon illumination by a focused vortex beam in a TEM. The particle was placed under the beam of $m = -1$ or $m = +1$ orders (marked by the arrows), which caused rotation in different directions. *Reproduced with permission from Verbeeck et al. (2013). Copyright by John Wiley and Sons. (See the color plate.)*

produced a vortex electron beam of $m = -1, 0, +1$ orders, with diameters down to the atomic level. The authors detected the rotation of an individual particle illuminated with a vortex beam. Moreover, the direction of the rotation depended on the diffraction order of the beam (i.e., $m = -1$ or $m = +1$, as shown in Figure 3.24). The observed effect was attributed to the transfer of an angular momentum from the vortex beam to the particle due to the electromagnetic interaction.



6. CONCLUSION

The electron microscope was initially invented as an instrument that could obtain images with a resolution higher than that in an optical microscope. However, a modern electron microscope is not just an imaging tool, but a complex analytical instrument or an advanced nanofabrication workstation. For either of these applications, the possibility for micromanipulation is greatly needed. In this chapter, we described three main methods of using micromanipulation in electron microscopes.

Mechanical (or contact) manipulation involves using an integrated micromanipulator for handling objects while the electron microscope

performs imaging. This method was introduced in 1990, and presently it allows not only manipulation with nanoscale precision, but also investigation of several mechanical properties of microobjects and nanoobjects that still are not well known. Other possibilities are electrostatic and electromagnetic noncontact manipulations, which are based on the intrinsic properties of an electron beam to deliver an electrical charge and create an electromagnetic field. The advantage of noncontact manipulation is that it can cause less potential damage to the transported object. Moreover, electromagnetic manipulation, which was experimentally demonstrated only a few years ago, offers the unique potential of precise transportation of nanometer-sized clusters, which is a very interesting phenomenon from both scientific and application points of view.

ACKNOWLEDGMENTS

This work was supported by the government of the Russian Federation (Grant # 074-U01) and the Russian Foundation for Basic Research (Grant # 14-02-31703).

REFERENCES

- Ampem-Lassen, E., Simpson, D. A., Gibson, B. C., Trpkovski, S., Hossain, F. M., Huntington, S. T., Ganesan, K., Hollenberg, L. C. L., & Prawer, S. (2009). Nanomanipulation of diamond-based single photon sources. *Optics Express*, *17*, 11287–11293.
- Ashkin, A. (1970). Acceleration and trapping of particles by radiation pressure. *Physics Review Letters*, *24*, 156.
- Batson, P. E., Reyes-Coronado, A., Barrera, R. G., Rivacoba, A., Echenique, P. M., & Aizpurua, J. (2011). Plasmonic nanobilliards: Controlling nanoparticle movement using forces induced by swift electrons. *Nano Letters*, *11*, 3388–3393.
- Batson, P. E., Reyes-Coronado, A., Barrera, R. G., Rivacoba, A., Echenique, P. M., & Aizpurua, J. (2012). Nanoparticle movement: Plasmonic forces and physical constraints. *Ultramicroscopy*, *123*, 50–58.
- Bergstrom, L. (1997). Hamaker constants of inorganic materials. *Advances in Colloid and Interface Science*, *70*, 126–169.
- Bussolotti, F., D’Ortenzi, L., Grossi, V., Lozzi, L., Santucci, S., & Passacantando, M. (2007). In situ manipulation and electrical characterization of multiwalled carbon nanotubes by using nanomanipulators under scanning electron microscopy. *Physical Review B*, *76*, 125415.
- Cagliani, A., Wierzbicki, R., Occhipinti, L., Petersen, D. H., Dyvelkov, K. N., Sukas, Ö. S., Herström, B. G., Booth, T., & Bøggild, P. (2010). Manipulation and in situ transmission electron microscope characterization of sub-100-nm nanostructures using a microfabricated nanogripper. *Journal of Micromechanics and Microengineering*, *20*, 035009.
- García de Abajo, F. J. (2004). Momentum transfer to small particles by passing electron beams. *Physical Review B*, *70*, 115422.
- Carpick, R. W., & Salmeron, M. (1997). Scratching the surface: Fundamental investigations of tribology with atomic force microscopy. *Chemical Reviews*, *97*, 1163–1194.
- Cazaux, J. (2004). Charging in scanning electron microscopy “from inside and outside.” *Scanning*, *26*, 181–203.

- Chen, X., & Wen, J. (2012). In situ wet-cell TEM observation of gold nanoparticle motion in an aqueous solution. *Nanoscale Research Letters*, 7, 598.
- Chen, Q., Smith, J. M., Park, J., Kim, K., Ho, D., Rasool, H. I., Zettl, A., & Alivisatos, A. P. (2013). 3D motion of DNA-AU nanoconjugates in graphene liquid cell electron microscopy. *Nano Letters*, 13, 4556–4561.
- Clévy, C., Hubert, A., Agnus, J., & Chaillet, N. (2005). A micromanipulation cell including a tool changer. *Journal of Micromechanics and Microengineering*, 15, S292–S301.
- Contreras-Naranjo, J. C., & Ugaz, V. M. (2013). A nanometre-scale resolution interference-based probe of interfacial phenomena between microscopic objects and surfaces. *Nature Communications*, 4, 1919.
- Cretu, O., Rodríguez-Manzo, J. A., Demortière, A., & Banhart, F. (2012). Electron beam-induced formation and displacement of metal clusters on graphene, carbon nanotubes, and amorphous carbon. *Carbon*, 50, 259–264.
- Denisyuk, A. I., Tinskaya, M. A., Petrov, M. I., Shelaev, A. V., & Dorozhkin, P. S. (2012). Tunable optical antennas based on metallic nanoshells with nanoknobs. *Journal of Nanoscience and Nanotechnology*, 12, 8246–8250.
- Denisyuk, A. I., Komissarenko, F. E., & Mukhin, I. S. (2014). Electrostatic pick-and-place micro/nanomanipulation under the electron beam. *Microelectric Engineering*, 121, 15–18.
- Derjaguin, B. V., Muller, V. M., & Toporov, Y. P. (1975). Effect of contact deformations on the adhesion of particles. *Journal of Colloid Interface Science*, 53, 314–326.
- Dong, L., Shou, K., Frutiger, D. R., Subramanian, A., Zhang, L., Nelson, B. J., Tao, X., & Zhang, X. (2008). Engineering multiwalled carbon nanotubes inside a transmission electron microscope using nanorobotic manipulation. *IEEE Transactions on Nanotechnology*, 7, 508–518.
- Ducker, W. A., Senden, T. J., & Pashley, R. M. (1991). Direct measurement of colloidal forces using an atomic force microscope. *Nature*, 353, 239–241.
- Egerton, R. F., Li, P., & Malac, M. (2004). Radiation damage in the TEM and SEM. *Micron*, 35, 399–409.
- Eichhorn, V., Fatikow, S., Wortmann, T., Stolle, C., Edeler, C., Jasper, D., Sardan, O., Boggild, P., Boetsch, G., Canales, C., & Clavel, R. (2009). NanoLab: A nanorobotic system for automated pick-and-place handling and characterization of CNTs. *Proceedings of IEEE International Conference on Robotics and Automation*, 1826–1831.
- Enomoto, K., Kitakata, S., Yasuhara, T., Ohtake, N., Kuzumaki, T., & Mitsuda, Y. (2006). Measurement of Young's modulus of carbon nanotubes by nanoprobe manipulation in a transmission electron microscope. *Applied Physics Letters*, 88, 153115.
- Fukata, N., Oshima, T., Tsurui, T., Ito, S., & Murakami, K. (2005). Synthesis of silicon nanowires using laser ablation method and their manipulation by electron beam. *Science and Technology of Advanced Materials*, 6, 628–632.
- Fukuda, T., Arai, F., & Dong, L. (2003). Assembly of nanodevices with carbon nanotubes through nanorobotic manipulations. *Proceedings of IEEE*, 91, 1803–1818.
- Fukuda, T., Arai, F., & Nakajima, M. (2013). *Micro-nanorobotic Manipulation Systems and Their Applications*. Berlin: Springer.
- Götzinger, M., & Peukert, W. (2003). Dispersive forces of particle-surface interactions: Direct AFM measurements and modeling. *Powder Technology*, 130, 102–109.
- Grobelyny, J., Tsai, D.-H., Kim, D.-I., Pradeep, N., Cook, R. F., & Zachariah, M. R. (2006). Mechanism of nanoparticle manipulation by scanning tunnelling microscopy. *Nanotechnology*, 17, 5519–5524.
- Hamaker, H. C. (1937). The London-van der Waals attraction between spherical particles. *Physica*, 4, 1058–1072.
- Hänel, K., Birkner, A., Müllegger, S., Winkler, A., & Wöll, C. (2006). Manipulation of organic “needles” using an STM operated under SEM control. *Surface Science*, 600, 2411–2416.

- Hatamura, Y., & Morishita, H. (1990). Direct coupling system between nanometer world and human world. *Proceedings of IEEE Micro Electro Mechanical Systems*, 203–208.
- Höppener, C., & Novotny, L. (2008). Imaging of membrane proteins using antenna-based optical microscopy. *Nanotechnology*, 19, 384012.
- Hu, S., Kim, T. H., Park, J. G., & Busnaina, A. A. (2010). Effect of different deposition mediums on the adhesion and removal of particles. *Journal of the Electrochemical Society*, 157, H662–H665.
- Jasper, D. (2011). *SEM-based motion control for automated robotic nanohandling*, Dr. rer. nat. dissertation. Oldenburg, Germany: Carl von Ossietzky University of Oldenburg.
- Jasper, D., & Fatikow, S. (2010). Automated high-speed nanopositioning inside scanning electron microscopes. *Proceedings of IEEE Conference on Automation Science and Engineering*, 704–709.
- Johnson, K. L., Kendall, K., & Roberts, A. D. (1971). Surface energy and the contact of elastic solids. *Proceedings of the Royal Society of London A*, 324, 301–313.
- Kasaya, T., Miyazaki, H. T., Saito, S., Koyano, K., Yamaura, T., & Sato, T. (2004). Image-based autonomous micromanipulation system for arrangement of spheres in a scanning electron microscope. *Review of Scientific Instruments*, 75, 2033–2042.
- Kim, K. S., Lim, S. C., Lee, I. B., An, K. H., Bae, D. J., Choi, S., Yoo, J.-E., & Lee, Y. H. (2003). In situ manipulation and characterizations using nanomanipulators inside a field emission-scanning electron microscope. *Review of Scientific Instruments*, 74, 4021–4025.
- Kim, S., Shafiei, F., Ratchford, D., & Li, X. (2011). Controlled AFM manipulation of small nanoparticles and assembly of hybrid nanostructures. *Nanotechnology*, 22, 115301.
- Krakov, W., & Nixon, W. C. (1977). The behavior of charged particles in the scanning electron microscope. *IEEE Transactions on Industry Applications*, IA-13, 355–366.
- Liu, K. H., Gao, P., Xu, Z., Bai, X. D., & Wang, E. G. (2008). In situ probing electrical response on bending of ZnO nanowires inside transmission electron microscope. *Applied Physics Letters*, 92, 213105.
- Mai, W., Zhang, L., Gu, Y., Huang, S., Zhang, Z., Lao, C., Yang, P., Qiang, P., & Chen, Z. (2012). Mechanical and electrical characterization of semiconducting ZnO nanorings by direct nano-manipulation. *Applied Physics Letters*, 101, 081910.
- Mayer, J., Giannuzzi, L. A., Kamino, T., & Michael, J. (2007). TEM sample preparation and FIB-induced damage. *MRS Bulletin*, 32, 400–407.
- Min, Y., Akbulut, M., Kristiansen, K., Golan, Y., & Israelachvili, J. (2008). The role of inter-particle and external forces in nanoparticle assembly. *Nature Materials*, 7, 527–538.
- Miyazaki, H., & Sato, T. (1996). Pick-and-place shape forming of three-dimensional micro structures from fine particles. *Proceedings of IEEE*, 2535–2540.
- Miyazaki, H. T., Tomizawa, Y., Koyano, K., Sato, T., & Shinya, N. (2000a). Adhesion force measurement system for micro-objects in a scanning electron microscope. *Review of Scientific Instruments*, 71, 3123–3131.
- Miyazaki, H. T., Tomizawa, Y., Saito, S., Sato, T., & Shinya, N. (2000b). Adhesion of micrometer-sized polymer particles under a scanning electron microscope. *Journal of Applied Physics*, 88, 3330–3340.
- Mølhave, K., Wich, T., Kortschack, A., & Bøggild, P. (2006). Pick-and-place nanomanipulation using microfabricated grippers. *Nanotechnology*, 17, 2434–2441.
- Nakajima, M., Arai, F., & Fukuda, T. (2006). In situ measurement of Young's modulus of carbon nanotubes inside a TEM through a hybrid nanorobotic manipulation system. *IEEE Transactions on Nanotechnology*, 5, 243–248.
- Nakazato, Y., Yuasa, T., Sekine, G., Miyazawa, H., Jin, M., Takeuchi, S., Ariga, Y., & Murakawa, M. (2009). Micromanipulation system using scanning electron microscope. *Microsystems Technology*, 15, 859–864.
- Neuman, K. C., & Block, S. M. (2004). Optical trapping. *Review of Scientific instruments*, 75, 2787–2809.

- Niguès, A., Siria, A., Vincent, P., Poncharal, P., & Bocquet, L. (2014). Ultrahigh interlayer friction in multiwalled boron nitride nanotubes. *Nature Materials*, *13*, 688–693.
- Oleshko, V. P., & Howe, J. M. (2011). Are electron tweezers possible? *Ultramicroscopy*, *111*, 1599–1606.
- Oleshko, V. P., & Howe, J. M. (2013). Electron tweezers as a tool for high-precision manipulation of nanoobjects. *Advances in Imaging and Electron Physics*, *179*, 203–262.
- Peng, L.-M., Chen, Q., Liang, X. L., Gao, S., Wang, J. Y., Kleindiek, S., & Taic, S. W. (2004). Performing probe experiments in the SEM. *Micron*, *35*, 495–502.
- Polyakov, B., Dorogin, L. M., Vlassov, S., Kink, I., Lohmus, A., Romanov, A. E., & Lohmus, R. (2011). Real-time measurements of sliding friction and elastic properties of ZnO nanowires inside a scanning electron microscope. *Solid State Communications*, *151*, 1244–1247.
- Polyakov, B., Vlassov, S., Dorogin, L. M., Kulis, P., Kink, I., & Lohmus, R. (2012). The effect of substrate roughness on the static friction of CuO nanowires. *Surface Science*, *606*, 1393–1399.
- Polyakov, B., Vlassov, S., Dorogin, L. M., Novoselska, N., Butikova, J., Antsov, M., Oras, S., Lohmus, R., & Kink, I. (2014). Some aspects of formation and tribological properties of silver nanodumbbells. *Nanoscale Research Letters*, *9*, 186.
- Reyes-Coronado, A., Barrera, R. G., Batson, P. E., Echenique, P. M., Rivacoba, A., & Aizpurua, J. (2010). Electromagnetic forces on plasmonic nanoparticles induced by fast electron beams. *Physical Review B*, *82*, 235429.
- Ru, C., & To, S. (2012b). Contact detection for nanomanipulation in a scanning electron microscope. *Ultramicroscopy*, *118*, 61–66.
- Ru, C., Zhang, Y., Huang, H., & Chen, T. (2012a). An improved visual tracking method in scanning electron microscope. *Microscopy and Microanalysis*, *18*, 612–620.
- Saito, S., Miyazaki, H. T., Sato, T., & Takahashi, K. (2002). Kinematics of mechanical and adhesional micromanipulation under a scanning electron microscope. *Journal of Applied Physics*, *92*, 5140–5149.
- Sitti, M., & Hashimoto, H. (2000). Controlled pushing of nanoparticles: Modeling and experiments. *IEEE/ASME Transactions of Mechatronics*, *5*, 199–211.
- Van Huis, M. A., Kunneman, L. T., Overgaag, K., Xu, Q., Pandraud, G., Zandbergen, H. W., & Vanmaekelbergh, D. (2008). Low-temperature nanocrystal unification through rotations and relaxations probed by in situ transmission electron microscopy. *Nano Letters*, *8*, 3959–3963.
- Verbeeck, J., Tian, H., & Van Tendeloo, G. (2013). How to manipulate nanoparticles with an electron beam? *Advanced Materials*, *25*, 1114–1117.
- Vlassov, S., Polyakov, B., Dorogin, L. M., Lohmus, A., Romanov, A. E., Kink, I., Gnecco, E., & Lohmus, R. (2011). Real-time manipulation of gold nanoparticles inside a scanning electron microscope. *Solid State Communications*, *151*, 688–692.
- Vlassov, S., Polyakov, B., Dorogin, L. M., Antsov, M., Mets, M., Umalas, M., Saar, R., Lohmus, R., & Kink, I. (2014). Elasticity and yield strength of pentagonal silver nanowires: In situ bending tests. *Materials Chemistry and Physics*, *143*, 1026–1031.
- White, E. R., Mecklenburg, M., Shevitski, B., Singer, S. B., & Regan, B. C. (2012). Charged nanoparticle dynamics in water induced by scanning transmission electron microscopy. *Langmuir*, *28*, 3695–3698.
- Williams, P. (1987). Motion of small gold clusters in the electron microscope. *Applied Physics Letters*, *50*, 1760–1762.
- Xu, S.-Y., Sun, W.-Q., Zhang, M., Xu, J., & Peng, L.-M. (2010). Transmission electron microscope observation of a freestanding nanocrystal in a Coulomb potential well. *Nanoscale*, *2*, 248–253.
- Ye, X. (2012). *Towards automated nanomanipulation under scanning electron microscopy*, Master of science thesis. Toronto, Canada: University of Toronto.

- Ye, X., Zhang, Y., Ru, C., Luo, J., Xie, S., & Sun, Y. (2013). Automated pick-place of silicon nanowires. *IEEE Transactions on Automation Science and Engineering*, 1–8.
- Yu, M., Dyer, M. J., Skidmore, G. D., Rohrs, H. W., Lu, X., Ausman, K. D., Von Ehr, J. R., & Ruoff, R. S. (1999). Three-dimensional manipulation of carbon nanotubes under a scanning electron microscope. *Nanotechnology*, 10, 244–252.
- Zhang, Y. L., Li, J., To, S., Zhang, Y., Ye, X., You, L., & Sun, Y. (2012). Automated nanomanipulation for nanodevice construction. *Nanotechnology*, 23, 065304.
- Zhang, Y. L., Zhang, Y., Ru, C., Chen, B. K., & Sun, Y. (2013). A load-lock-compatible nanomanipulation system for scanning electron microscope. *IEEE/ASME Transactions on Mechatronics*, 18, 230–237.
- Zheng, Q., Jiang, B., Liu, S., Weng, Y., Lu, L., Xue, Q., Zhu, J., Jiang, Q., Wang, S., & Peng, L. (2008). Self-retracting motion of graphite microflakes. *Physics Review Letters*, 100, 067205.
- Zheng, H., Mirsaidov, U. M., Wang, L.-W., & Matsudaira, P. (2012). Electron beam manipulation of nanoparticles. *Nano Letters*, 12, 5644–5648.
- Zonneville, A. C., Hagen, C. W., Kruit, P., & Schmidt-Ott, A. (2009). Directed assembly of nano-particles with the help of charge patterns created with scanning electron microscope. *Microelectric Engineering*, 86, 803–805.